

EE 241 Final Report

Ultra-smooth platinum films for biosensing applications

Charmaine Chia | SNF staff: Michelle Rincon | Mentors: Karl Littau, Don Gardner

CONTENTS		pg
Executive Summary		2
I. Motivation and approach		3
II. Chemical Mechanical Polishing		4
A. Description of approach		4
B. Results and observations		4
III. Patterned Template Stripping		6
A. Description of approach		6
B. Process development & results		7
C. Issues encountered		9
D. Tips and tricks		10
IV. Sputtering & Annealing		11
A. Description of approach		11
B. Results and observations		12
1) Observations from depositions of 1x1 cm ² samples		12
2) Observations from depositions on 4" wafers		14
C. Tips and tricks		16
V. Comparison and Functionalization tests		16
A. AFM and SEM images		16
B. Functionalization tests		16
1) Self-assembled monolayer functionalization		17
2) Gold nanoparticle functionalization		17
VI. Conclusions		18
VII. References		18
VIII. Acknowledgements.....		18
Appendix 1: Table of samples deposition conditions		19
Appendix 2: Table of SEM and XRD measurements on all samples deposited		20

EXECUTIVE SUMMARY

Aim: To prepare platinum films of < 1 nm RMS roughness. Such a film could be useful in improving the uniformity, yield and performance of molecular electronics and plasmonic devices, which have critical length scales on the same order. Additionally, the film should be stable against thermal treatment (up to 300 °C) and organic solvents.

Chemical Mechanical Polishing

- Polishing parameters:
 - ❖ Polishing head pressure: 150 g/cm²
 - ❖ Polishing pad pressure: 250 g/cm²
 - ❖ Pad rotation: 50 rpm
 - ❖ Head rotation: 30 rpm
 - ❖ Polishing time: < 2 min
- Slurry:
 - ❖ Dissolve periodic acid in DI water to a concentration of 10 mM

Add 2 parts DI water (with periodic acid added) to 1 part slurry, as obtained from SNF. Either Ultra-Sol S10 or 2EX is fine.

Patterned Template stripping

- Pattern template wafer (Si prime), with desired pattern to be transferred *not* exposed
 - Resolution down to 20 μm comfortable; for smaller features depends on aspect ratio of feature (sensitivity to shearing)
- DRIE etch (~ 8 μm deep)
- Deposit 10 nm Cr / 8 nm Au
- Overnight liftoff in acetone, *gentle* sonication if needed, IPA clean
- Piranha clean (5 min, 3:1 piranha)
- Deposit 70 – 100 nm Pt / 8 nm Ti. If thick film, maybe allow break for film to cool to avoid delamination
- Plasma clean of glass wafer
- Spin SOG 400F @ 2000 rpm, 30 s
- Place glass wafer facedown onto template, clamp (not too hard!!)
- Cure for 1h @ 120 °C, 1h @ 200 °C

Allow wafer stack to cool; separate with scalpel

Sputter deposition + annealing

- Quartz wafer
- Acetone + IPA rinse, blowdry, then plasma clean in Plasm-Etcher (next to Lesker) for ~ 3 min
- Deposition conditions:
 - ❖ KJ Lesker, room temperature
 - ❖ Adhesion layer: Ti @ 200 W, 3 mTorr, 50 sccm Ar / 5 sccm O₂, 5 min
 - ❖ Film: Pt @ 170 W, 6 mTorr, 50 sccm Ar / 6 O₂ (10.7%), room temperature, 30 min
- Anneal conditions:
 - ❖ Tylan9, recipe M1000: 1000 °C for 1 h

I. Motivation and approach

Metallic thin films are typically deposited by evaporation or sputtering, resulting in a polycrystalline morphology with a preferred orientation. As nanotechnology shrinks devices to the dimensions of individual crystal grains and the research community explores alternative nanomaterials for electronic devices, such as DNA, organic molecules, nanotubes and nanoparticles, the variations and discontinuities introduced by grain boundaries are becoming increasingly relevant technologically. Grain boundaries determine a material's mechanical strength electrical and properties, acting as scattering centers and possible paths of current leakage. They are also crucial to its surface properties, introducing both roughness and regions of higher surface energy owing to its nature as an accumulation of defects. This in turn leads to defects in self-assembled monolayers (SAM) functionalized onto the metal surface (Fig. 1a), as well preferential attachment of nanoparticles within grain boundaries (Fig. 1b)—undesirable if a uniform and dense coverage is the goal.

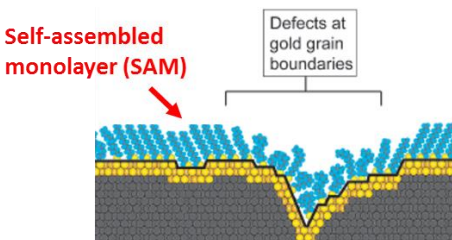


Fig 1a: Defects in an SAM due to grain boundaries

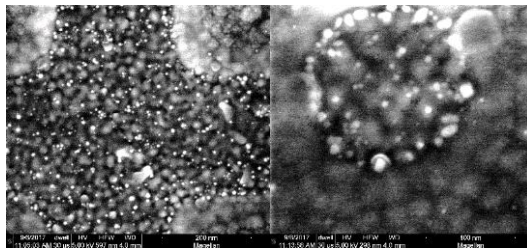


Fig. 1b: Preferential deposition of nanoparticles in grain boundaries

For applications ranging from molecular electronics to biosensing and plasmonics, being able to control the smoothness of a metallic thin film could thus bring huge improvements in performance, yield and reproducibility of nanoscale devices. In this project, I explore different approaches to achieve this with platinum as the metal of choice. Ultra-smooth metal films have been achieved with oblique ion milling, chemical mechanical polishing (CMP) and template stripping, while grain boundary reduction has been achieved through epitaxial single crystal growth, annealing, and deposition of metallic glass. In view of the tools at our disposal, my focus will be on the methods of **1) CMP**, **2) template stripping** and **3) sputter deposition followed by annealing**.

Several protocols have been reported for platinum for these methods. However, further process development is needed to adapt them to the tools and materials we have at our disposal in the SNF and Exfab, and to meet unique specifications for my intended application. CMP on platinum was described more than a decade ago; however due to limited demand, there is currently no commercial slurry targeting platinum, most instead catering to Si, SiO₂, W and Cu, which are much less chemically inert. In template stripping, the metal film is deposited onto an atomically flat substrate like silicon or mica, then transferred to the actual substrate via a bonding layer.⁶ This is most commonly a UV-curable adhesive (e.g. Norland 81), which has the advantages of being easy to lay down (via spin coating) and cure. However, it is difficult to transfer large areas of metal with this method; importantly, the adhesive often has a relatively low glass transition temperature (< 100 °C) and limited solvent resistance, placing constraints on subsequent processing. Metallic / eutectic bonding has been shown to be a viable alternative for transferring metal films from templates. However this method requires use of a wafer bonding tool at high temperatures and pressures to achieve the bonding, and also precludes the transfer of pre-patterned films from the template. In this case, it means the platinum has to be patterned by ion milling after its transfer, a method which is not very scalable with our current fab facilities. Finally, a process for the growth of giant grains of Pt by sputtering with added oxygen, followed by a high temperature anneal, was reported and subsequently applied as a substrate to grow large areas of graphene.¹⁰ However, it is known that sputter deposition parameters depend strongly on the tool being used, and furthermore 'abnormal grain growth' is only observed within a narrow window of parameters, and may thus require some experimentation to achieve on the KJ Lesker sputter tool.

In the following sections, work done on the above 3 techniques will be described and their results compared. The objective, simply, is to lay down a metallic film of platinum with atomic level (< 0.5 nm) roughness. If possible, variation in the surface energy landscape would also be minimized by reducing the presence of grain boundaries. The film morphology should also be thermally stable upon further processing for several hours up to 250 °C, and

also be chemically stable to Standard Clean 1 (SC1), as well as solvents like ethanol, acetone, and dichloromethane. Finally, consideration will be given to the scalability of the procedure given the constraints of the present fab facilities. The ultimate application goal is to pattern a wafer-scale array of electrodes based on the platinum films developed, and subsequently to functionalize a well-packed, low defect film of alkanedithiol onto the platinum, to which gold nanoparticles (10 nm diameter) will attach in a uniform monolayer of high density.

II. Chemical Mechanical Polishing (CMP)

A. Description of approach

Chemical mechanical polishing is a process of smoothing surfaces with the combination of chemical and mechanical forces. The process uses an abrasive and corrosive chemical slurry (commonly a colloid) in conjunction with a polishing pad and retaining ring, typically of a greater diameter than the wafer. The pad and wafer are pressed together by a dynamic polishing head and held in place by a plastic retaining ring. During polishing, both the polishing head and pad are rotated (with different axes and speeds of rotation), while a lateral oscillation is also applied to the polishing head to encourage movement of slurry. This process removes material and tends to even out any irregular topography, making the wafer flat or planar. Generally, polishing pads are made from porous polymeric materials with a pore size between 30 and 50 μm .

Typical materials polished with CMP include silicon and silicon dioxide, as well as interconnect materials like copper, aluminum, tungsten, and more recently, carbon nanotubes. While slurries have been developed for noble metals like gold, silver and platinum, these generally have low removal rates due to the chemical inertness of these metals (especially platinum), and are generally not commercially available due to their limited industrial use. In 2005, Islam et al reported a two-step CMP process for platinum that achieved a roughness of 0.1 nm with low defectivity.¹ However, the proprietary alumina slurry they used by Dupont-EKC comprising a mixture of ZCX-206 and oxidizer ZCX-206B in a ratio of 3:7, was an experimental line back then and is no longer available. Thus, developing a CMP process for platinum will require a different slurry made from currently available products.

B. Results and observations

Several slurry formulations were tested based on slurries available in the SNF: Ultra-sol S10 and Ultra-sol 2EX. Both these slurries have alkaline pH and silica colloidal nanoparticles around 70 nm in size, and come in 30% solids form. S10 is designed for polishing silicon, while 2EX is designed for silicon dioxide. Nevertheless, it was reported by previous users that polishing was possible with a silica based slurry, even if mostly mechanical. Based on recommendations from CMP experts, slurries with *hydrogen peroxide* and *periodic acid* as oxidizing agents were also tested, diluted to 5% and 10% solids respectively.² Fig. 3 and 4 show the results of AFM scans on 150 nm evaporated Pt samples polished with the S10 and 2EX-based formulations, respectively. Row 1 shows the $5 \times 5 \mu\text{m}^2$ scans, row 2 shows the $1 \times 1 \mu\text{m}^2$ scans, and row 3 the $200 \times 200 \text{ nm}^2$ scans.

The following parameters were standardized for the tests: The polishing head pressure was 150 g/cm^2 (2.13 psi), while the pad pressure was 250 g/cm^2 . The pad and head rotation were 50 rpm and 30 rpm respectively. Polish time was 2 minutes. After polishing, the wafer was rinsed with DI water and immediately placed into a beaker of water for transfer to the wash area, where it was then rinsed with water from the gooseneck while wiping it down with a wet clean wipe. The purpose of this is to remove remaining slurry particles on the wafer before it the wafer dries and they become stuck. (Evidence of poor cleaning can be seen in Fig. 3i.) Between wafers, the pad should also be kept wet to prevent slurry particles drying on it, which could result in scratches.

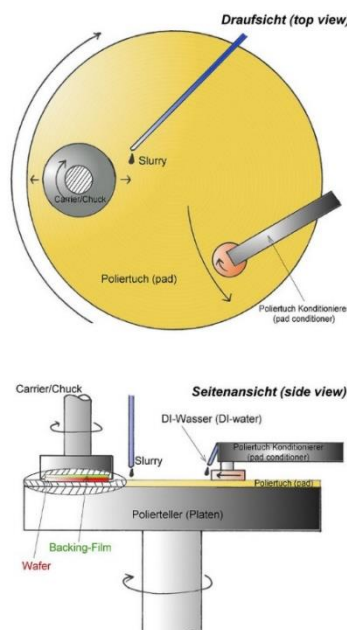


Fig. 2: Top and side views of CMP setup

Fig. 3: AFM images taken after CMP on evaporated Pt film with various slurries based on Ultra-etch S10

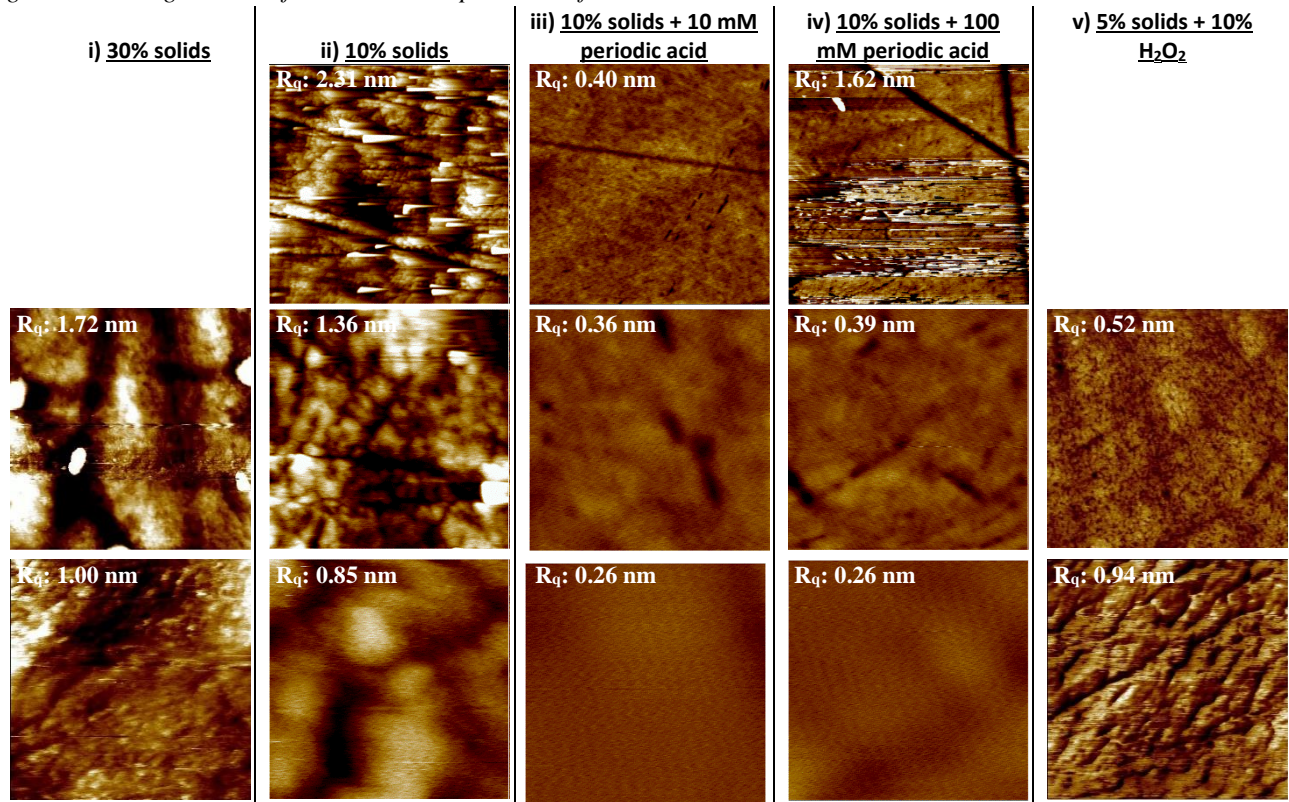
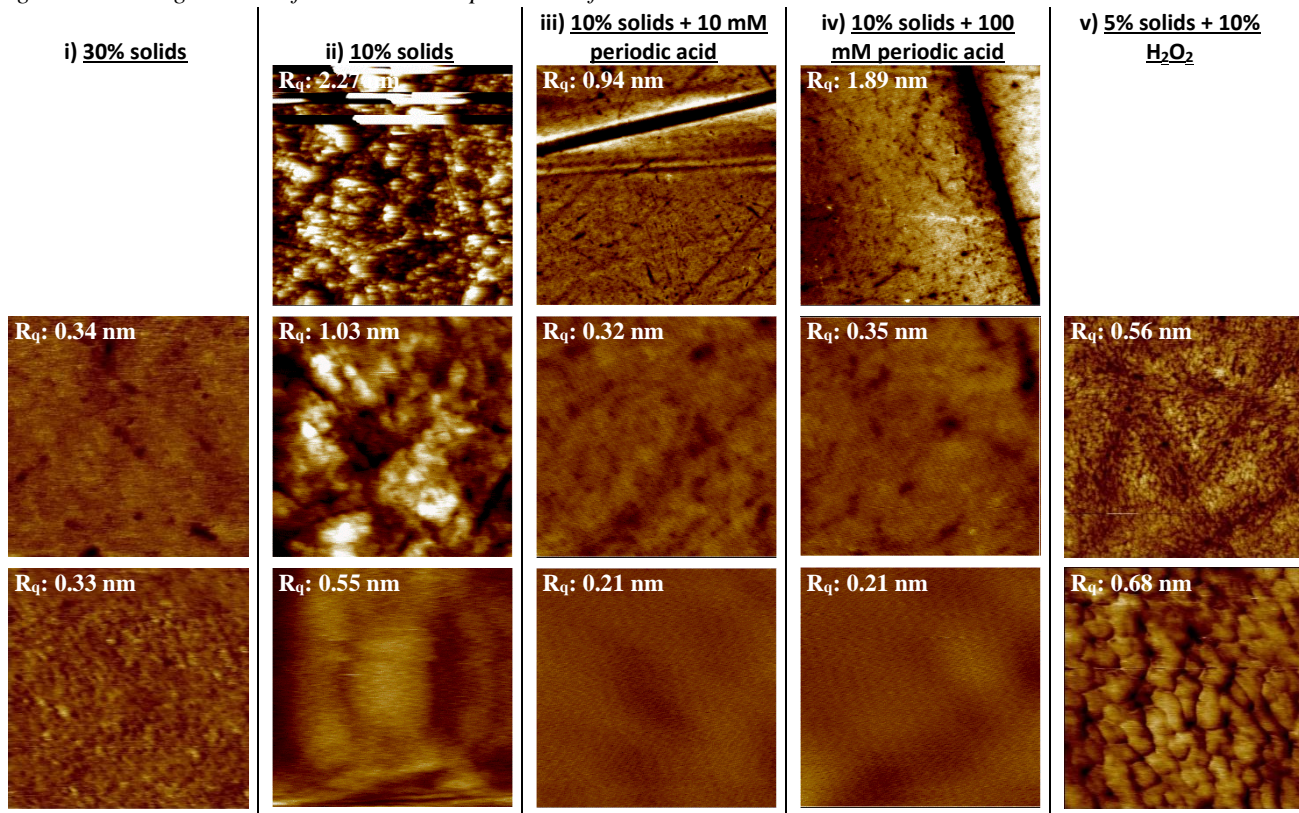


Fig. 4: AFM images taken after CMP on evaporated Pt film with various slurries based on Ultra-etch 2EX



Scratches were observed on all the wafers after polishing; however, the depth and frequency of scratches varied from wafer to wafer. This is a common problem with CMP, and future work can focus on reducing defectivity by optimizing over pressure and polish time, or perhaps by splitting the polishing up into two parts. Nevertheless, for our purposes, some amount of scratching is tolerable as long as the film is smooth on a 100 nm scale.

This appears to be the case for the films polished with formulations (i) 30% solids, (iii) 10% solids + 10 mM periodic acid, and (iv) 10% solids + 100 mM periodic acid, although the frequency of scratches is lower for (iii) than (iv). Comparing splits (ii) with (iii), we see that the addition of periodic acid in (iii) does aid in polishing, and the resulting films retain less trace of their original granularity than the controls (ii). Overall, it the most promising slurry formulations are 10% solids with 10 mM periodic acid, giving an RMS roughness of 0.36 nm.

Future work could explore alternative colloids for the slurry such as ceria or alumina, the former of which gives better surface finish, and the latter of which is harder than silica and may yield a higher removal rate (although this may also increase defectivity). The wafers could also be cleaned in SC1 after polishing for better contamination removal.

III. Patterned Template Stripping

A. Description of approach

Template stripping was first developed to obtain ultra-smooth unpatterned metal films, making use of the poor adhesion and good wettability of noble metals on solids such as mica and silicon. Typically, freshly cleaved mica is coated with a film of gold, and the exposed surface of gold is then attached to another substrate with an optical epoxy adhesive. When the mica and substrate are separated, the gold clings to the epoxy, and a metal interface that has formed on the mica is exposed. Because mica can be extremely smooth, ultraflat gold surfaces can be generated. These have been used widely in scanning probe experiments and studies of self-assembled monolayers. Building on this method, several groups have produced metal films with 3D structures like grooves, pyramids and apertures using pre-patterned silicon templates, demonstrating devices with much enhanced plasmonic and SERS performance.³⁻⁵ This technique is promising for the application targeted here; unfortunately, it needs to be adapted to a different adhesive which meets my stability specifications, and also be capable of transferring fine structures across the area of a 4-inch wafer. Most reported transfers so far have been on a few-cm scale.

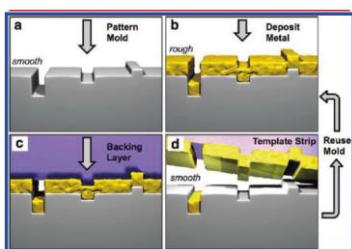


Figure 1. Processing schematic. (a) A silicon mold is first prepared for template stripping bumps, grooves, and apertures. (b) Subsequent metal deposition forms a smooth interface with the silicon, though the backside of the as-deposited metal is rough. (c) By attaching a backing layer such as epoxy, (d) the entire metal film, transferred with the patterning, is stripped. Forming apertures requires that the deposited film is discontinuous.

Fig. 5a: Template stripping process

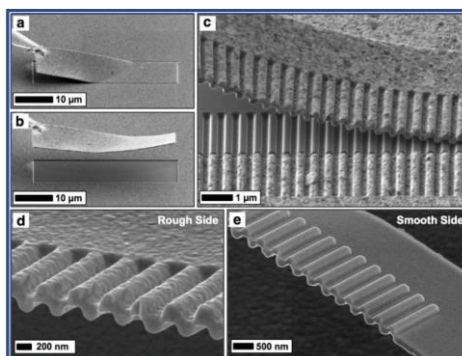


Fig. 5b: Example of top and bottom side of template stripped surface

A possible alternative to optical epoxies is a silica-based adhesive. Sodium silicate, also known as liquid glass, is a compound that is soluble in water and forms a thermally resistant glassy solid upon curing. Used as an adhesive, a refractory binder, drilling fluid, automotive finishing, etc, it was also explored as a solvent-resistant adhesive for template stripping, in a process shown below.⁷ However, testing out this process, I observed severe cracking and fragmentation of the metal film after curing of the template-metal-substrate stack, which may have been caused by shrinkage of the liquid glass upon curing. In fact, even without curing, the liquid glass film spun onto the substrate seems to automatically de-wet as it dried, forming intricate dendritic patterns rather than a uniform adhesive layer. This may have been due to the substrate and metal surfaces not being hydrophilic enough; however, even a 10 minute treatment in O₂ plasma did not rectify this condition. Furthermore, liquid glass seems

to form relatively thick layers ($\sim 8 \mu\text{m}$) upon spin-coating, which results in the substrate becoming stuck to the template even in areas where it is not supposed to, making it hard to separate them without breakage.

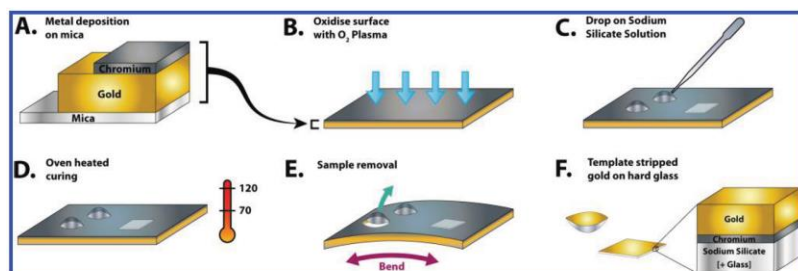


Figure 1. IgTSG fabrication schema. (A) Gold (150 nm) and chromium (5 nm) layers are thermally evaporated onto a freshly cleaved mica substrate. (B) Chromium is hydrophilically functionalized by oxygen plasma. (C) Sodium silicate solution (liquid glass) is drop cast onto the chromium surface. Plasma-cleaned glass slides can be placed on top of these droplets to form a sturdier backing. (D) Heating in a two-stage process balances water evaporation and transformation to silica. (E) IgTSG can easily be removed by gently bending the mica. (F) The process results in ultraflat gold backed onto a glass slide or a thin ($300 \mu\text{m}$) silica sheet.

Fig. 6: Template stripping using liquid glass



Fig. 7: Wafer stack after curing process, using with liquid glass as adhesive

B. Process development & results

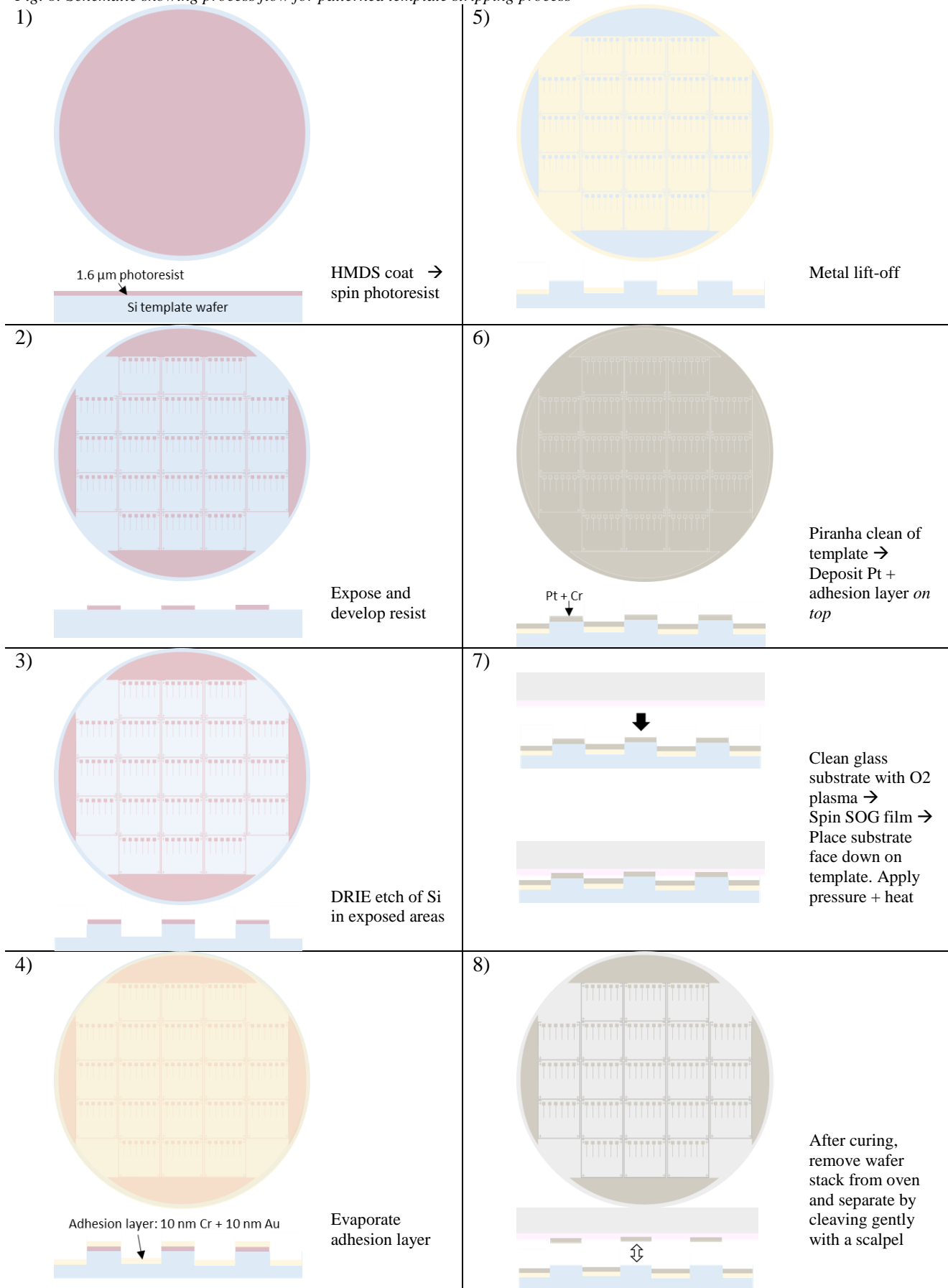
To overcome this, I looked into a spin-on glass (SOG), a class of silicon-based polymer that can be cured to form networks that are stable up to high temperatures. These include silicates, which form a network of $[\text{SiO}_2]_n$, as well as variants with some carbon content, like methylsiloxanes $[\text{H}_3\text{CSiO}_2]_m[\text{SiO}_2]_{n-m}$ and methylsilsesquioxanes $[\text{H}_3\text{CSiO}_{3/2}]_n$, which generally have increased cracking resistance and lower shrinkage upon curing, and better planarization properties. SOG 400F, a methylsilsesquioxane-based polymer, was chosen due to its superior cracking properties and availability in the SNF. This forms a layer of $\sim 400 \text{ nm}$ when spun at 2000 rpm.

A process for the template stripping transfer of pre-patterned films was devised as shown in Fig. 8. The general idea is to etch a relief into the template wafer, with the desired electrode pattern raised above the surrounding areas like in a woodblock stamp. The first metal deposition followed and lift-off will coat the low-lying areas with an adhesion layer, while the second deposition will cover the raised electrode pattern with the Pt to be transferred. The steps are:

- 1) After standard cleaning of the template wafer, coat with HMDS and spin $1.6 \mu\text{m}$ of 3612 resist.
- 2) Expose and develop resist with electrode array pattern, with resist in non-electrode areas removed
- 3) Etch Si in exposed areas with DRIE to a depth of $\sim 10 \mu\text{m}$.
- 4) *Deposit a thin metal adhesion layer (10 nm Cr + 10 nm Au) by evaporation.
- 5) Overnight lift-off in acetone (double bath, with slight sonication at the end) followed by IPA rinse to remove metal on electrode areas.
- 6) Piranha clean of substrate to remove all residual organics. Deposit Pt layer ($\sim 70 \text{ nm}$) followed by thin Cr or Ti adhesion layer ($\sim 8 \text{ nm}$) by evaporation.
- 7) Clean glass substrate with acetone + IPA followed by O_2 plasma treatment. Spin 400F SOG at 2000 rpm for 30s. Then immediately place substrate wafer facedown onto template, and apply uniform pressure and heat (in oven or on hotplate).
- 8) After curing period, separate the wafer stack carefully using a scalpel blade.

A one-step deposition (i.e. Pt followed by Cr) was initially tested, and resulted in a film that delaminated from the low-lying areas very easily even when external pressure was not applied, giving an *inverse* of the pattern desired. This was unexpected, as these regions lay some $10 \mu\text{m}$ further away from the glass substrate than the raised electrode pattern, where the metal was *not* transferred to the glass substrate (Fig. 9). Film transfer of the electrode patterns was only achieved with the introduction of the adhesion layer (step 4) to keep the metal surrounding the desired pattern stuck to template. In addition, significant pressure needed to be applied to get high yield. The challenge then was to prepare a setup that would be able to apply this pressure to the wafer stack while allowing it to be heated to up to $200 \text{ }^\circ\text{C}$ to cure the SOG film.

Fig. 8: Schematic showing process flow for patterned template stripping process



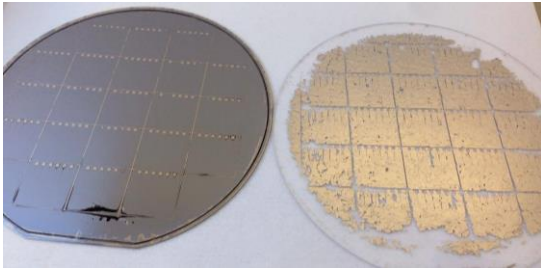


Fig. 9: One-step deposition with inverse transfer

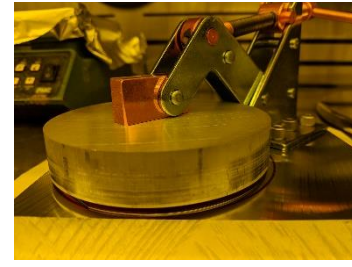
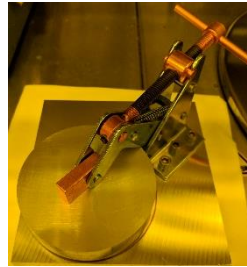


Fig. 10: Top and side view of custom clamp setup

The setup designed comprises a 6" square, 3/4" thick cast aluminum tooling plate, onto which a hold down toggle clamp was mounted with high-temperature / high-strength steel screws. To apply pressure onto the template-substrate wafer stack, a piece of 3.75" diameter silicone rubber is placed on top of it, followed by a 4" diameter, 3/4" thick 6061 aluminum alloy disc. The disc and silicone rubber piece help apply uniform pressure across the wafer stack.

Curing was once the wafer stack is securely clamped into place by placing the clamp setup into the oven and heating up to 120 °C for 1 h, followed by 200 °C for 1 h. Fig. 11 shows images taken from the process, along with micrograph examples of successfully transferred regions. Eventually, complete transfer of the large features (down to 20 μm) on all 21 die on the wafer was achieved. However, reliable transfer of fine features (2 μm) still remains a challenge, as described in the next section.

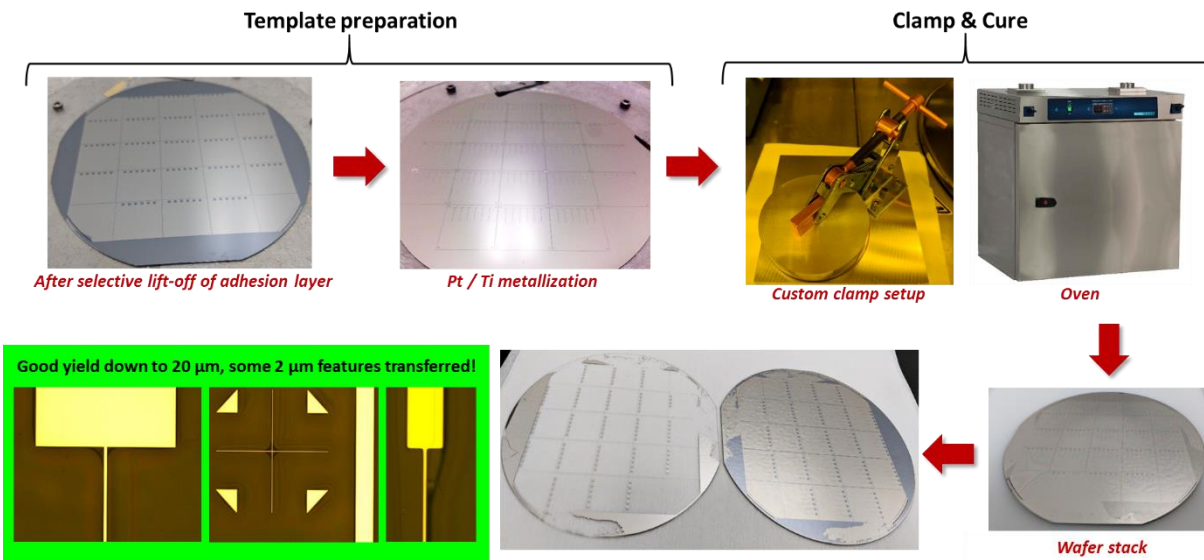


Fig. 11: Images from template stripping process with SOG 400F

C. Issues encountered

Several issues were encountered and the process was iterated with changes each time to try and fix the problems. Among these were:

It.	Process description	Issue	Cause
1	4" square steel blocks used to apply pressure.	Incomplete transfer: ~70% yield of large patterns	Insufficient / non-uniform pressure
2	Switched to custom clamp for applying pressure.	Fine structures (2 μm crosses and wires) were not transferred	Collapse of fine structures
3	Etch depth: 19 μm	Arc of adhesion layer (10 nm Ti / 5 nm Pt) removed during piranha clean before second deposition	Ti is etched by piranha, esp since Pt overlayer is relatively thin

4	Etch depth: 10 μm	2 μm crosses transferred, but 2 μm wide, 2.5 mm long wires appeared sheared to various degrees across the wafer	TBD in next few iterations
5	Lipped template to enable wafers to be separated with minimal shear	“	<u>Not</u> due to shear forces during wafer separation
6	Etch depth: 1 μm	Wafers were stuck together	
7	Etch depth: 8 μm 10 μm wide wires (instead of 2 μm)	10 μm wide wires were still sheared at the very end, though less severely than 2 μm wires in previous iterations. However, template structures remained intact	Shearing <u>not</u> due to collapse of structures

An important aspect of the process design is the tradeoff between mechanical stability of the fine template structures and the separation between desired pattern in relief its background, controlled by the etch depth. This is illustrated in Fig. 12a. Too high an aspect ratio (> 5 or so, or $> 10 \mu\text{m}$ etch depth for a $2 \mu\text{m}$ wide wire) resulted in structures collapsing easily when vigorous sonication was applied. However, when the etch depth was decreased to $1 \mu\text{m}$, the template and substrate wafer ended up stuck together at the portions that were covered the adhesion layer, making them impossible to separate without breakage.

Substrate stuck to template Collapse of fine template structures

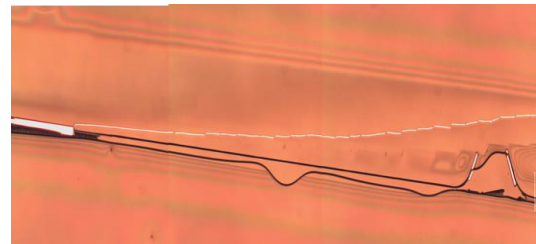
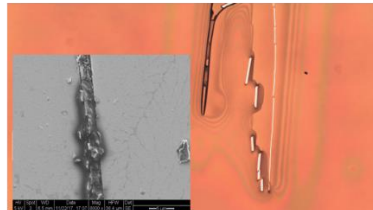
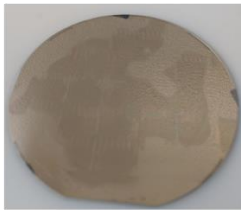


Fig. 12a: Tradeoff between etch depth and structural stability

Fig. 12b: Shearing of fine wire structure

The second main issue was the shearing of fine $2 \mu\text{m}$ wire structures on most of the dies on the wafer save for a select few (Fig. 12b). Shearing during the wafer separation stage and template structure collapse were ruled to be independent of this phenomenon by performing simple controls in iterations 5 and 7. The most plausible remaining explanation is that differential pressure on either side of the fine wires caused them to drift to one side during the curing process, much as one might squeeze toothpaste down a tube by applying more pressure at one end. This was further supported by the appearance of more complete metal transfer on the side of the wafer the wires were sheared *away* from, suggesting more pressure was applied on that side. Unfortunately, this issue of uneven pressure application is not easily solved with the current custom setup, which does not provide for a good means of aligning to wafer stack such that the clamp head rests square in its center. Moreover, the clamp mechanism shows signs of slight wobbling from side to side as it is screwed down. If available, a wafer bonding tool would be ideal for this, and would allow the pressure applied to be measured as well for more systematic and reproducible processing.

E. Tips and tricks

- For thicker films, the Pt metal deposition may be better done in two parts so thermal stress does not build up and cause metal to delaminate right after deposition.
- Wafer flatness should be checked as any curvature may introduce shear stress in the wafer stack.
- Use a gentle sonication for liftoff is necessary to avoid collapse of fine wire features.
- A piranha (or plasma) clean is needed after liftoff to ensure the template surface is very clean and smooth
- Use Cr / Au for the adhesion layer – these etch slower in piranha compared respectively to Ti / Pt.
- After spinning of the SOG layer on the glass substrate, template and substrate should be brought together swiftly to avoid the SOG layer drying, which would compromise the adhesion to the metal to be transferred.

IV. Sputtering & annealing

A. Description of approach

The aim of this approach is to control the morphology of the platinum film to achieve giant grains. This was reported to be possible by introducing oxygen gas during sputter deposition onto SiO₂/Si substrates, encouraging the as-deposited film have random rather than (111) orientation as is typical. The incorporated oxygen on reduces the surface mobility of Pt adatoms and introduces compressive stress into the lattice, causing (111) to no longer be the most energetically favorable orientation for the atoms to arrange into. Subsequent annealing above 750 °C for 1 h in ambient was found to induce transformation of the platinum films into giant grains on the order of millimeters, via abnormal grain growth (AGG).¹⁰⁻¹³

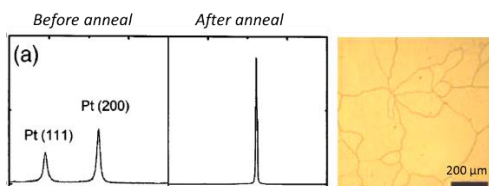


Fig 13a: XRD measurement before and after anneal for film deposited at 5 mTorr, 15% O₂

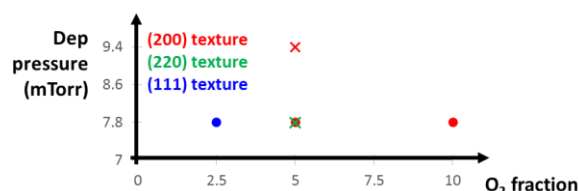


Fig. 13b: Preferred orientation of films for various sputter conditions (from literature), after 1 h anneal 1000 °C

Fig. 13a shows an XRD measurement on a sample before and after annealing, when the all the grains were converted to (200) orientation. Fig. 13b summarizes sputter conditions (pressure, O₂ fraction) given in the two studies that reported giant grains after annealing. These data points have been color coded according to the texture of the final films—all three textures, (200), (220), and (111) were observed, in one case with supposedly identical deposition conditions. It is speculated that the strain minimization through driving out of trapped oxygen during annealing is what induces giant grain growth, but a mechanism explaining how different post-anneal textures develop under different conditions has yet to be put forth.

Depositions in the Exfab were done on the KJ Lesker tool, and annealing was done in the tube furnace Tylan9 in 80-20 N₂-O₂ atmosphere. Quartz was chosen as the substrate for its high temperature resistance and compatibility with application needs (low impedance), with most depositions done on sample chips diced to a dimension of 1 x 1 cm² (with a protective layer of resist spun before dicing). Before use, the resist was removed by an acetone and IPA rinse, blow-dried, and plasma cleaned in the plasma-etch tool for 2 minutes. The samples were then attached to the Lesker substrate holder using a clip on one corner.

Initial deposition conditions attempted to reproduce results from published sputter parameters, starting with 9.4 mTorr and 4.8% O₂ fraction – to achieve this, the argon gas flow was kept constant at 50 sccm, and O₂ gas flow set to 5 sccm. However, this did not result in giant grains upon annealing and instead gave a matte-looking film (Fig. 14). Subsequent depositions explored process parameters around this to obtain the desired outcome, and giant grain growth was eventually achieved. In general, the following conditions were observed:

Parameters kept constant	Parameters varied
<ul style="list-style-type: none"> Substrate DC power Adhesion layer: TiO₂ (200 W, 3 mTorr, 50 sccm Ar / 5 sccm O₂, 5 min) Pt deposition time (30 min) Anneal temperature (1000 °C) Anneal time (1 h) 	<ul style="list-style-type: none"> Sputter pressure (5 – 9.4. mTorr) O₂ fraction (2 – 11.5%) Deposition temperature

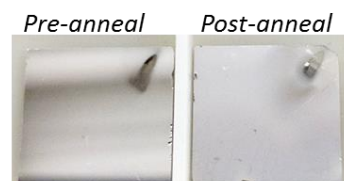


Fig. 14: Starting sample before and after anneal

SEM and XRD measurements were done on the samples before and after annealing to determine the morphology and texture of the film. Electron Backscattering Diffraction (EBSD), a spatially resolved crystal orientation measurement technique, was also done on selected samples to map between microstructure and crystal orientation.

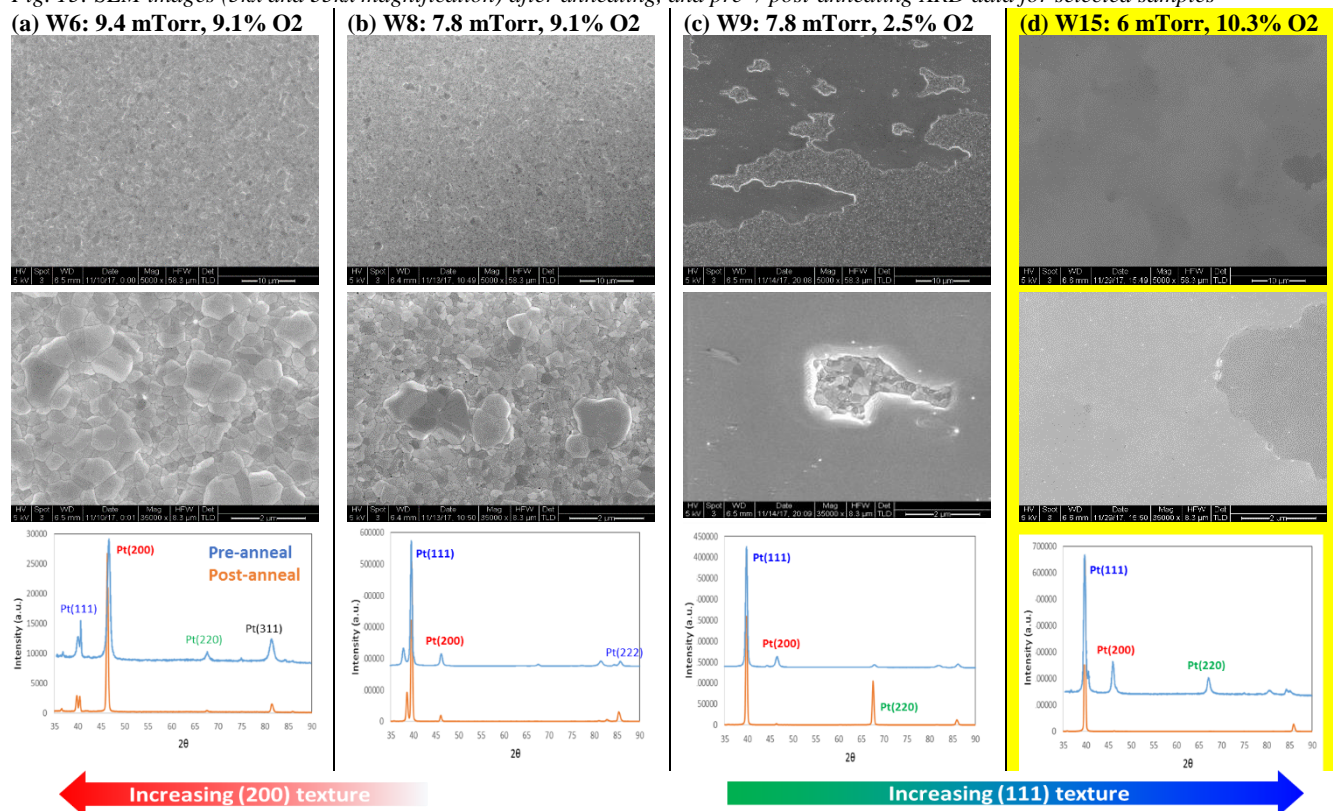
Appendix 1 shows a list of all the sample depositions done, along with processing conditions. Appendix 2 shows a tabulation of the SEM, XRD and EBSD measurements done, arranged by deposition pressure and O₂ fraction, to aid in observing trends along as parameters are varied along these dimensions.

B. Results and observations

1. Observations from depositions on 1x1 cm² samples

As mentioned, the very first deposition parameters attempted (9.4 mTorr, 4.8% O₂) resulted in a matte-looking film after annealing. Using SEM imaging, the cause of this was readily found to be microstructural roughness arising from a bimodal distribution of grain sizes, wherein courser grains (2–5 μm) were embedded within a matrix of smaller grains (200–500 nm). This is a result of abnormal grain growth, which is characterized by a subset of grains growing at a high rate and at the expense of their neighbors owing to some advantage like increased strain energy as a driving force or enhanced mobility. However, the continued presence of the smaller grains attests to the fact that the competition between normal (driven by minimization of grain boundary energy) and abnormal grain growth has not yet become dominated by the latter. Indeed, most of the samples emerged from the furnace anneal looking dull and matte, immediately indicating the desired complete giant grain growth was not achieved. The degree of bimodality in the rough-looking samples varied with deposition parameters, with the large grains being closer or further in size relative to the small grains, and occurring with different densities.

Fig. 15: SEM images (5kx and 35kx magnification) after annealing, and pre- / post-annealing XRD data for selected samples



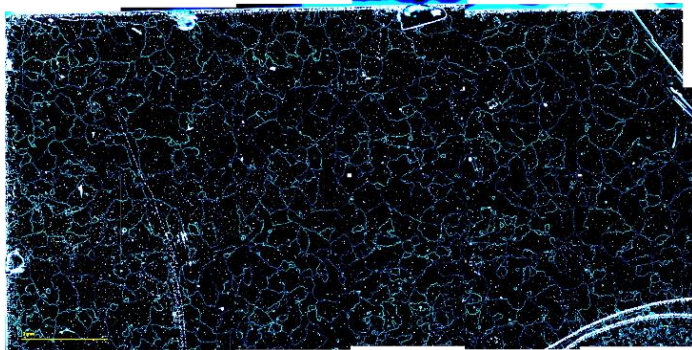
In Fig. 15, we see examples of post-anneal samples exhibiting a range of microstructure. Bimodal grain size distribution can be seen in Fig. 15a, b & c, with increasing starkness. In Fig. 15d, the morphology has become entirely dominated by giant grains, which cover hundreds of microns in extent. This suggests that giant grain growth is an extreme case of bimodal grain growth, achieved when the conditions not only allow the large grain growth to not only outstrip that of the small grains, but also to persist and eventually eliminate the smaller grains

from the landscape. The XRD measurements in the 3rd row show how the as-deposited (blue) and post-anneal (orange) microstructure evolves with changing deposition conditions. The (111) peak in Pt occurs at around 39.76°, the (200) peak at 46.23°, the (220) peak at ~ 68°, and the (311) peak at 81.25°. From this and the complete tabulation of results in Appendix 2, the following trends might be observed:

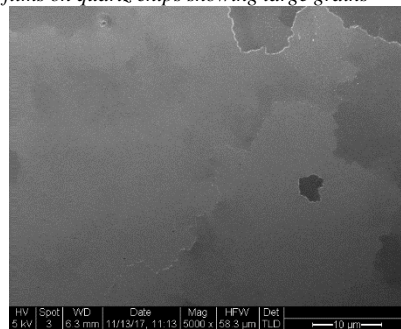
- a) **Effect of O₂ fraction and deposition pressure:** In general, as the O₂ fraction and pressure increases, the degree of (111) texture in as-deposited (pre-anneal) films decreases, leading to an increase of intensity of the (200) peak relative to the (111) peak. The increased gas pressure reduces the energy of impinging Pt atoms and might result in a less compact film with more oxygen incorporation.
As oxygen incorporation increases to approach conditions that would enable giant grain growth, we observe the large grains getting larger, producing an intermediate morphology as seen in Fig. 15c. When the optimal O₂ fraction (e.g. 11% @ 6 mTorr, 2.5% @ 7.8 mTorr) is exceeded, the film abruptly transforms into a matrix of small grains again, with sparsely distributed medium sized grains (see W10, W17 in Appendix 2).
- b) **Effect of deposition temperature:** Increasing the deposition temperature seems to result in a higher *density* of large grains after annealing. In the case where giant grains already dominate, a higher temperature seems to encourage more grains to nucleate simultaneously, resulting in smaller giant grains, as seen from the comparison between Fig. 16b and c. The increased availability of energy during deposition for Pt atoms to reorganize could promote a microstructure that favors large grain nucleation and growth in the annealing stage. SEM images suggest that such as-dep films have larger grains, and possibly a less (111) dominated texture, either of which could be a contributing factor. Alternatively, the increase in thermal stress in the as-deposited film could have encouraged the nucleation and growth of large grains upon annealing.
- c) **Effect of anneal time and temperature:** Different anneal times (1, 2h) and temperatures (850, 1000 °C) were tested for selected samples. No significant differences were observed in post-anneal morphology, suggesting that above a certain temperature and time, the microstructural transformation ‘saturates’.
- d) **Effect of film thickness:** For one set of deposition conditions which yielded giant grain growth after annealing (6 mTorr, 9.1% O₂), a split was done with the Pt deposition time halved. While the thinner film (Fig. 16e) shows budding signs of large grain growth, but it appears that a certain critical thickness is required for giant grains to take over (Fig. 16d). Extrapolating from this, it may be possible to increase the size of the giant grains observed in Fig. 16d by increasing deposition time further from 30 minutes.
- e) **Effect of interfacial layer:** Another split was done for the 6 mTorr, 9.1% O₂ deposition condition in which the addition of oxygen during the Pt deposition phase was delayed by 100 s (this was after the deposition of the TiO₂ adhesion layer, effectively introducing a Pt seed layer where oxygen is not incorporated). This resulted in the inhibition of giant grain growth upon annealing, suggesting that the film transformation and extent of AGG is highly sensitive to the interfacial layer. The mediating factor may be the unfavorable film stress due to the interfacial layer, or the seeding of (111) texture by the interfacial layer. Indeed, XRD measurements show that the ratio of intensity of the (200) to (111) peak is 21% lower in the as-deposited film with the delayed introduction of O₂.
- f) **Effect of film stress:** Studies on the effect of film stress are tricky because variables that change film stress (e.g. temperature, deposition pressure) often modify some other property of the film, making it difficult to isolate the cause of an effect observed. Furthermore, direct measurements of film stress are difficult. Nevertheless, examples of non-uniform morphology across a single sample suggest that it could be an important factor determining film transformation. This makes intuitive sense since we speculate that AGG is driven by film stress due to incorporated oxygen. In Fig. 16b, we can observe how the density of giant grains is much higher towards the bottom-right of the image; in Fig. 16e, we see that large grains have developed extensively in the regions of buckling, while remaining relatively sparse in the surrounding film. Since the sample only ranges 1x1 cm², the as-deposited composition and temperature experienced in the furnace is not expected to vary much across the film. However, the film stress could vary, for example as a function of

distance to the edge of the sample or proximity to a region of buckling where the compression in the film is relieved, and might explain why some region of the film contain more large grains than others.

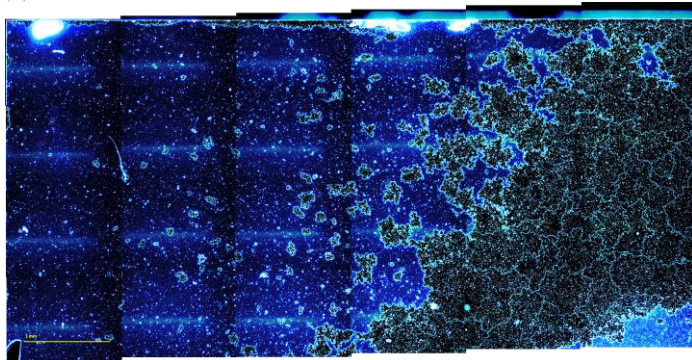
Fig. 16: Dark-field optical images (a, b, c) and SEM images (d, e, f) of post-anneal films on quartz chips showing large grains



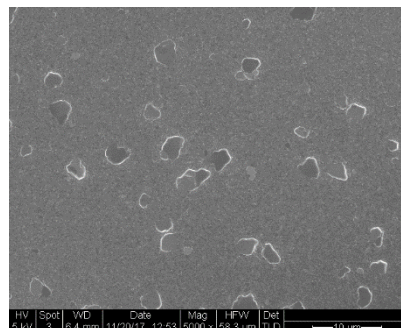
(a) W7: 6 mTorr, 9.1% O₂, 1000 °C 1 h anneal



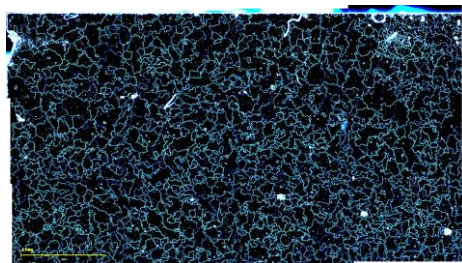
(d) W7: 6 mTorr, 9.1% O₂, **30 min** deposition. 1000 °C 1 h anneal



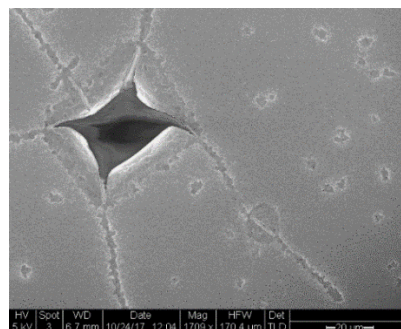
(b) W12: 7.8 mTorr, 2% O₂, 1000 °C 1 h anneal



(e) W11: 6 mTorr, 9.1% O₂, **15 min** deposition. 1000 °C 1 h anneal



(c) W13: 7.8 mTorr, 2% O₂, 80 °C deposition. 1000 °C 1 h anneal



(f) W2: 7.8 mTorr, 4.8% O₂, 1000 °C 1 h anneal

Overall, observations on how microstructure after annealing varied with O₂ fraction and pressure were roughly consistent with literature reports. However, while the publications did not mention the effect of film stress, this seems to play a significant role, and might possibly explain why giant grain growth was not obtained under exactly the same conditions. (Note, the substrate used here differs from that used in the reported studies is different and may subtly affect film stress; it is also possible that the sputter parameters are not directly comparable due to differences in the deposition systems.) In our depositions, large grain growth was observed primarily in (111) texture—referring back to Fig. 13b, this seems to correspond with the lower oxygen incorporation depositions reported. (220) texture in a film demonstrating intermediate morphology (W9); however, varying the O₂ fraction slightly above and below the value of 2.5% used in this deposition failed to produce a film composed solely of giant (220)-oriented grains. Finally, giant grain growth was *not* observed in the (200) texture. It is possible that the different substrate used here limits giant grain growth in these orientations; but it may yet be that further experimentation could uncover parameters delivering the ideal morphology in all three textures.

2. Observations from depositions on 4” wafers

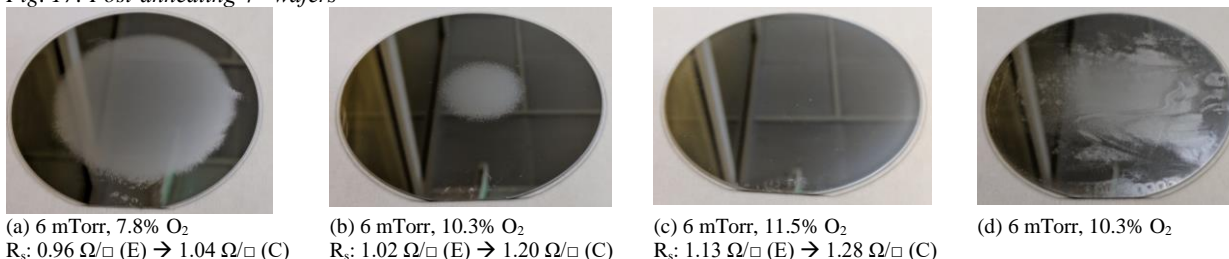
Having found several sets of deposition conditions that resulted in giant grain growth on chips after annealing at 1000 °C for 1 h, we proceeded to test the scalability of the method by repeating these depositions on 4” quartz

wafers. The wafers were placed vertically in a wafer boat, concentric with the furnace tube. Interestingly, the post-anneal morphology varied substantially across the wafer in a radial fashion, as seen from the appearance of a circular matte patch in the center of the wafers in Fig. 17a and b.

Possible sources of the non-uniform post-anneal morphology can be divided into two groups – non-uniformity present before the annealing step, and non-uniformity arising during annealing. These could include:

Non-uniformity in as-deposited film	Non-uniformity during annealing
i. Variation in thickness ii. Variation in oxygen incorporated iii. Variation in microstructure (e.g. grain size) iv. Variation in film stress (likely to be function of above parameters), along with thermal stresses due to substrate-film thermal coefficient mismatch	i. Variation in temperature within tube ii. Variation in film stress as the wafer is heated

Fig. 17: Post-annealing 4" wafers



From sheet resistance measurements at various positions of the as-deposited film, it was found that the resistivity is consistently higher in the center than the edges by about $0.15 \Omega/\square$, a significant fraction of the overall sheet resistance (on the order of $1 \Omega/\square$). It is unlikely that such variations can be explained by thickness changes, which are expected to be 1 – 2% for this deposition setup. This was backed up by profilometer measurements across the wafer. Other possibilities include variation in the amount of oxygen incorporated and/or microstructural variations, with smaller grains in the center (resulting in higher sheet resistance) and larger grains at the edges where grain growth is less constrained. However, verification of this requires further studies (SEM, XRD). Even if a correlation could be drawn between grain size and sheet resistance variation across the film, this does not necessarily confirm that the post-annealing non-uniformity arises from these variations.

Evidence that the post-anneal morphology is affected by how the wafer is placed in the tube was afforded by a split in which, a wafer was lain flat atop of a quartz slab (Fig. 18b). This caused a different matte pattern to emerge on the wafer after the anneal. As shown in Fig. 17d, the matte circle in the center has been replaced by a messy linear patch, suggesting that how heat is applied, and possibly the secondary effect on film stresses, does directly impact morphology evolution. Having said that, it has yet to be conclusively established whether radial temperature variation across the wafer in the vertical position are indeed the cause of the circular matte pattern.

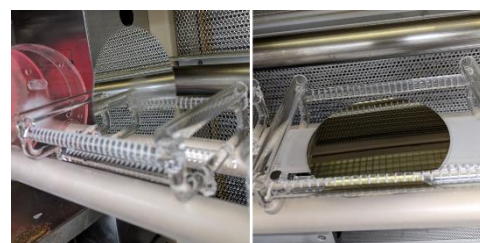


Fig. 18: Vertical and horizontal placement of wafer in furnace tube

One quirk that could be used to uncover whether this causal relationship exists is the observation that the circular matte pattern is actually off-center relative to the exact center of the wafer—i.e. shifted to the right and up (Fig. 17a and b). Interestingly, this shift is not affected by the orientation of the wafer flat in the furnace boat, suggesting that it is not caused by misalignment of the boat within the tube, and may be instead a function of deposition non-uniformity, or the way stress develops upon annealing due to the geometry of the wafer with the flat.

To obtain a film which was fully transformed to giant grains by annealing, different O_2 fractions were tested, and it was found that the size of the matte circle decreases as the O_2 fraction is increased between 7.8% to 11.5%,

after which bimodal grain growth occurs. An ideal set of deposition parameters might then be: 6 mTorr, 11% O₂, 30 minute deposition. The film thickness was measured to be around 300 nm.

C. Tips and tricks

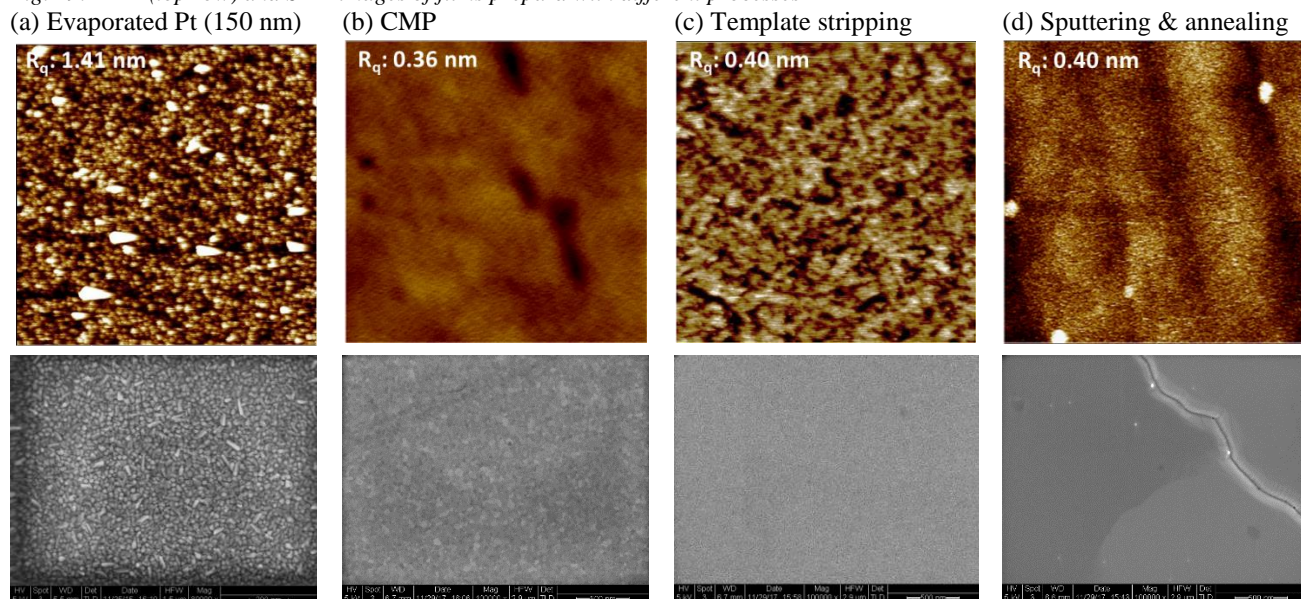
- The film transformation appears to be very sensitive to adhesion layer, possibly due to the stress it applies on the film, or the effect of seeding subsequent microstructure development, so this should be carefully monitored. Adhesion layer should also be thick enough (~20 nm) to avoid film cracking or delamination.
- Wafer cleaning could also affect the adhesion and stress in the film, which would affect morphology. Do a plasma clean right before deposition.
- Film composition is very sensitive to base pressure and this should be kept roughly constant for all depositions (ensure it is < 5e-7 mTorr).
- Monitor deposition temperature as well, as this affects as-deposited microstructure and stress, which in turn affects the microstructure after annealing.

V. Comparison & functionalization tests

A. AFM and SEM characterization

AFM (1x1 μm²) and SEM images (2.9 μm Horizontal Field Width) of the films prepared using the 3 approaches are shown in Fig. 19, alongside images for a 150 nm thick Pt film prepared in the standard way – e-beam evaporation. AFM suggests a roughness decrease from 1.41 nm to ~ 0.40 nm for all 3 approaches. While reasonably good, other studies have individually reported smoother films using template stripping and CMP, suggesting room for improvement. The SEM images of the CMP and template stripped film show some roughness, but these look different from the initial rounded grain structure.

Fig. 19: AFM (top row) and SEM images of films prepared with different processes



B. Functionalization experiments

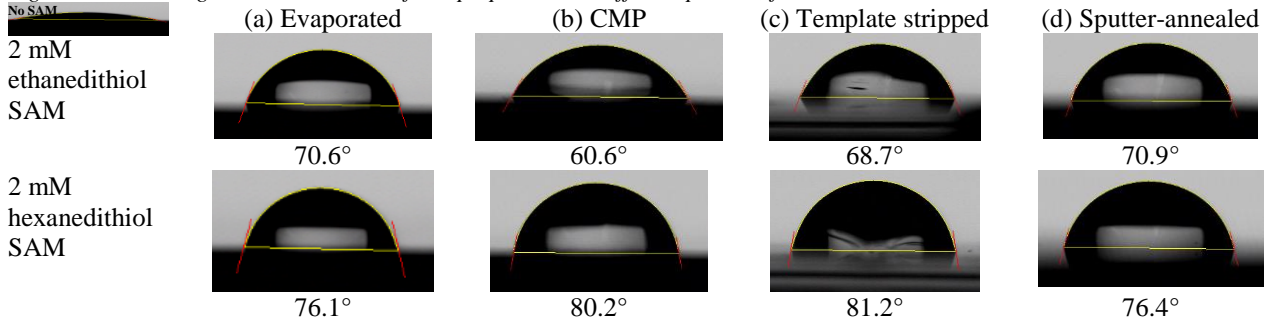
Finally, film samples from all 3 approaches were functionalized as intended in a future application—by immersion in a 2 mM solution of dithiol to form a self-assembled monolayer, followed by immersion in a gold nanoparticle solution, to encourage binding of the nanoparticles to the exposed end of the dithiol SAM. The presence of the SAM can be indicated by an increase in water contact angle (due to the hydrophobicity of the SAM). The gold nanoparticles can be visualized with SEM, although resolution becomes limited for very small nanoparticles.

1. Self-assembled monolayer (SAM) functionalization

Samples were cleaned in 5:1:1 SC1 solution (DI water:H₂O₂:NH₄OH) at 70 °C for 45 s, then rinsed in DI water and blow-dried in N₂. Next, they were rinsed in ethanol and then incubated in a 2 mM ethanolic solution of (a) ethanedithiol or (b) hexanedithiol. The thiol group is bonds covalently to platinum. After 24 h, the samples were taken out and sonicated in ethanol for 1 minute followed by a rinse to remove physisorbed molecules, then blow-dried. Water contact angle measurements were done on half the samples, with results as shown in Fig. 20.

The contact angle measurements were relatively consistent across the 2 different functionalizations for Pt films prepared in different ways, generally ranging from ~60 – 70° for ethanedithiol and ~75 - 80° for hexanedithiol. This suggests that hexanedithiol forms a higher quality SAM, causing the surface to appear more hydrophobic. This effect is well known: the greater length of the hexanedithiol (n = 6) molecule encourage a more ordered SAM to form, whereas the ethanedithiol molecule is speculated to form bilayers.

Fig. 20: Contact angle measurements on films prepared with different process, functionalized with 2 mM EDT or HDT

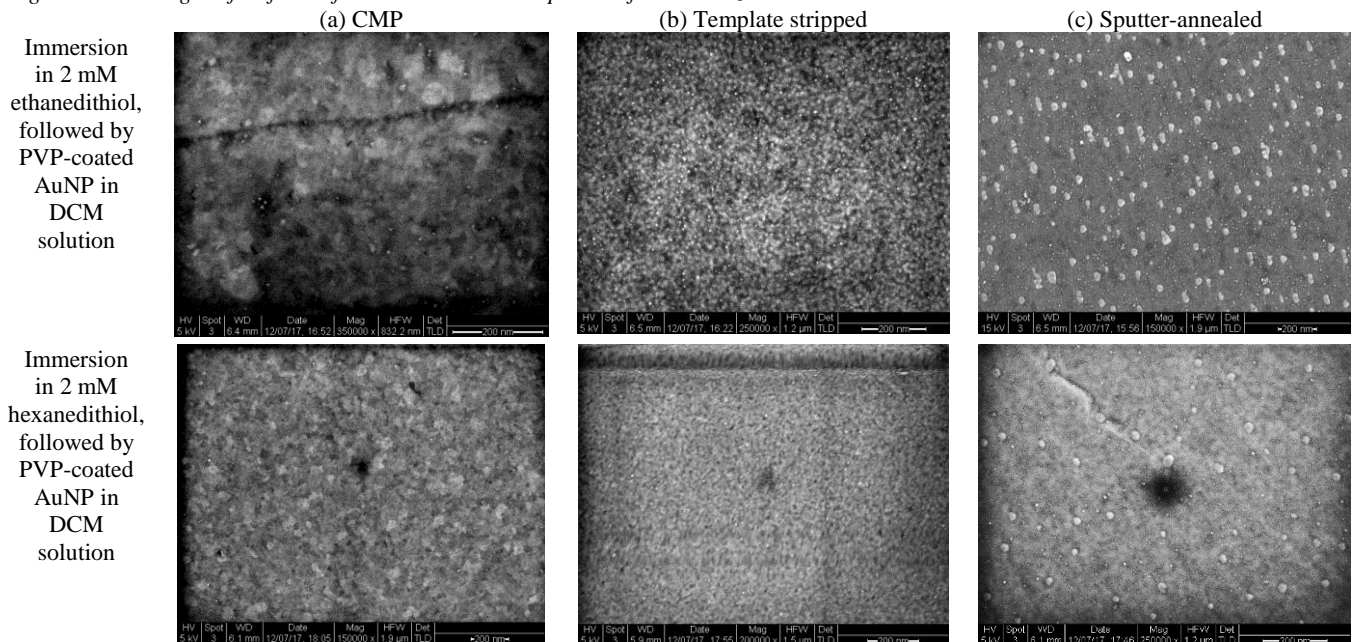


2. Gold nanoparticle functionalization

Nanoparticle solution preparation was done as follows. The PVP-coated gold nanoparticles were obtained in dried form from Nanopartz. They were reconstituted in dichloromethane (DCM) by first adding a few drops of isopropanol (IPA) to 2 mg of dried nanoparticles in a vial, then adding 2 ml of DCM and sonicating for 2 minutes to dissolve. Then, 6 ml of DCM was added to make up 8 ml in total.

Half of the SAM-functionalized samples were subjected to nanoparticle functionalization by individually immersing them (by tweezers) into the vial containing the nanoparticle solution. After 60 s, the sample would be taken out and rinsed in ethanol to get rid of agglomerates, then blow-dried. These samples were then imaged with SEM, as shown in Fig. 21.

Fig. 21: SEM images of Pt films after SAM and Au nanoparticle functionalization



If scrutinized carefully, one might observe small bright dots (~ 7 nm in diameter) against the darker background of the substrate in all the SEM images below. These are the gold nanoparticles, and their presence indicates successful functionalization. Unfortunately, resolution and contrast of the images is not good enough to determine the density of the nanoparticles. Imaging can be improved in the future by using slightly larger nanoparticles, a better SEM tool (Magellan instead of Sirion), and doing an in-situ plasma clean to shake off some of the SAM on the sample, which contributes to image distortion due to its insulating nature.

VI. Conclusions

3 different approaches to obtaining ultra-smooth platinum films were tested, with the following results:

- 1) Chemical mechanical polishing was able to achieve RMS roughness below 0.4 nm, with best results obtained with periodic acid added. Further work is likely to be able to bring roughness and defectivity down by optimizing over polish time, pressure and multi-steps.
- 2) A process was developed for patterned template stripping of sparse patterns, with good yield down to features of 20 μm . The adhesive is a silica-based spin-on polymer, which has much better temperature and solvent resistance (after curing) than conventional optical adhesives used. This process is scalable and the templates can be reused. Resolution can be improved with a more uniform pressure application setup, as well as a method to align the wafers together.
- 3) Parameters were found that yielded giant grains on the order of 100s of μm upon annealing. The study also yielded insights into how various deposition and annealing parameters affect film microstructure.

VII. References

1. Islam M. S. et al. 2005. Ultra-smooth platinum surfaces for nanoscale devices fabricated using chemical mechanical polishing. *Applied Physics A* 80: 1385–1389.
2. Kinoshita M. 2007. Slurries for CMP. In: Marinescu I, Uhlmann E, Doi T, editors. *Handbook of Lapping and Polishing*. 2nd ed. Florida (FL). CRC Press. p.370 – 395.
3. Nagpal P. et al. 2009. Ultrasmooth patterned metals for plasmonics and metamaterials. *Science* 325(5940): 594–597.
4. Lindquist N. et al. 2014. Template fabricated plasmonic nanoholes on analyte-sensitive substrates for real-time vapor sensing. *RSC Advances* 4: 15115–15121.
5. Lindquist N. et al. 2011. Monolithic integration of continuously tunable plasmonic nanostructures. *Nano Letters* 11: 3526–3530.
6. Vogel N. et al. 2012. As flat as it gets: ultrasmooth surfaces from template-stripping procedures. *Nanoscale* 4: 3820.
7. Hugall J. et al. 2012. Solvent-resistant ultraflat gold using liquid glass. *Langmuir* 28: 1347–1350.
8. Hashiguchi H. et al. 2014. A new temporary bonding technology with spin-on glass and hydrogenated amorphous Si for 3D LSIs. *ICEP Proceedings TA1-1*: 74–77.
9. Kim T. I. et al. 2014. Thin film receiver materials for deterministic assembly by transfer printing. *Chemistry of Materials* 26: 3502–3507.
10. Choi J. K. et al. 2015. Growth of wrinkle-free graphene on texture-controlled platinum films and thermal-assisted transfer of large-scale patterned graphene. *ACS Nano* 9(1): 679–686.
11. Kim M. H. et al. 1998. Highly (200)-oriented Pt films on SiO₂/Si substrates by seed selection through amorphization and controlled grain growth. *Journal of Materials Research* 14(3): 634–637.
12. Kim M. H. et al. 1998. Changes in preferred orientation of Pt thin films deposited by dc magnetron sputtering using Ar/O₂ gas mixtures. *Journal of Materials Research* 14(4): 1255–1260.
13. Lee D. S. et al. 2001. Preferred orientation controlled giant grain growth of platinum thin films on SiO₂/Si substrates. *Japanese Journal of Applied Physics* 40: L1.
14. Birnbaum A. J. et al. 2017. Oxygen-induced giant grain growth in Ag films. *Applied Physics Letters* 111: 163107.
15. Kabla M. et al. 2014. The relationships between sputter deposition conditions, grain size, and phase transformation temperatures in NiTi thin films. *Acta Materialia* 70: 79–91.
16. Miller D. et al. 2013. Giant secondary grain growth in Cu films on sapphire. *AIP Advances* 3: 082105.
17. Zielinski E. M. et al. 1995. The influence of strain energy on abnormal grain growth in copper thin films. *Applied Physics Letters* 67: 1078.
18. Moriyama M. et al. 2003. The Effect of Strain on Abnormal Grain Growth in Cu Thin Films. *Journal of Electronic Materials* 32(4): 261–267.

VIII. Acknowledgments

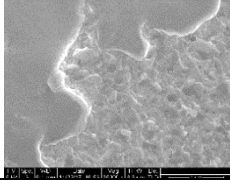
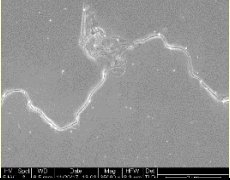
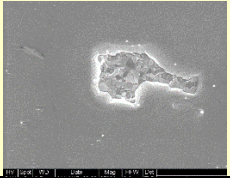
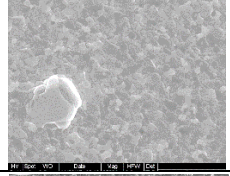
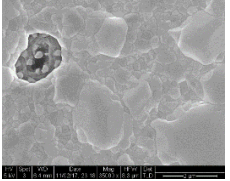
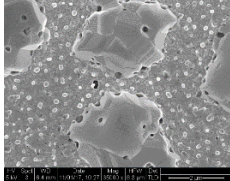
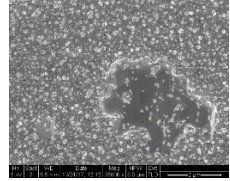
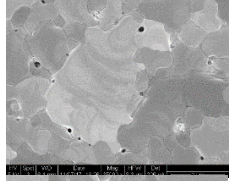
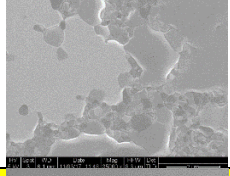
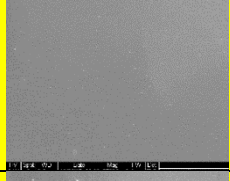
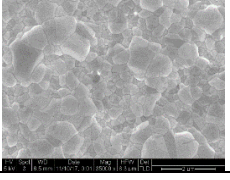
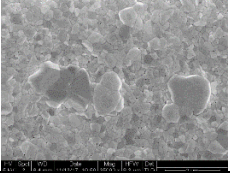
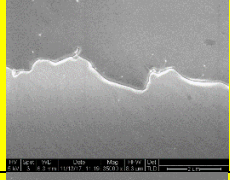
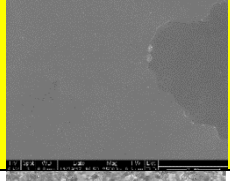
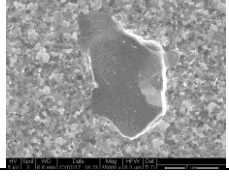
I would like to thank the following people for their invaluable advice and support:

- Mentors: Michelle, Karl, Don
- SNF: Maurice, Carsen, Mike, Swaroop, Usha, Mahnaz, Mary
- SNSF: Tom Carver, Shiva Bhaskaran
- Peter Schindler, Prof Sriniraghavan
- Prof. Fan and Andrew and Prof. Howe

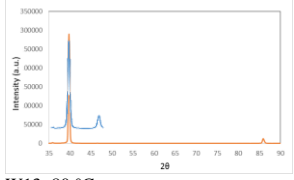
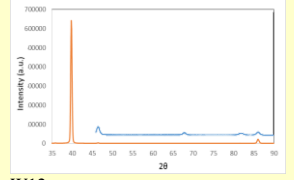
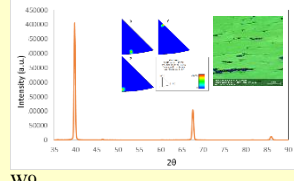
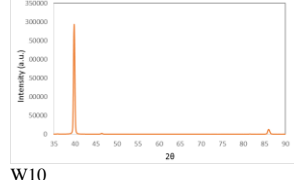
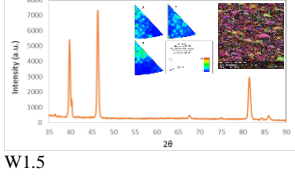
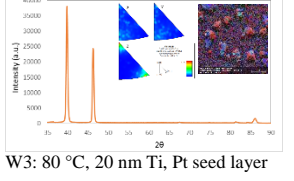
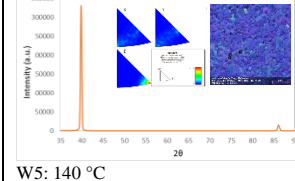
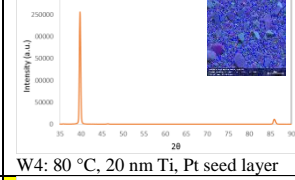
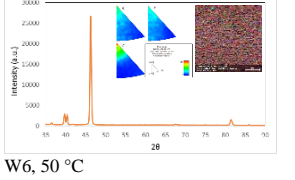
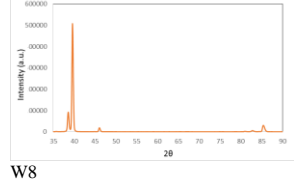
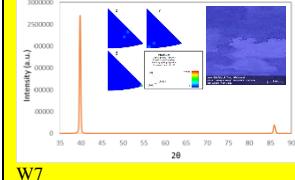
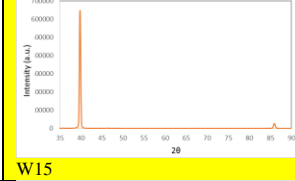
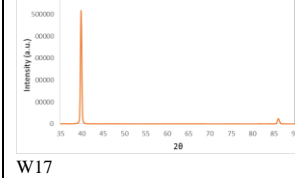
Appendix 1

Date	#	Substrate	Adhesion layer	Pt film
10/16	W1	Si/SiO ₂ , 1x1 cm ²	Ti, 200W / 3 mTorr / 1 min ~ 5 nm	170 W / 9.4 mTorr / 4.8% O ₂ / 30 min
10/17	W1.5	Quartz, 1x1 cm ²	Ti, 200W / 3 mTorr / 1 min ~ 5 nm	170 W / 9.4 mTorr / 4.8% O ₂ / 30 min
10/23	W2	Quartz, 1x1 cm ²	Ti, 200W / 3 mTorr / 4 min ~ 20 nm	170 W / 7.8 mTorr / 0% O ₂ / 0.5 min ⇒ 170 W / 7.8 mTorr / 4.8% O ₂ / 15+15min
10/31	W3	Quartz, 1x1 cm ² 80 -> 65 C	Ti, 200W / 3 mTorr / 4 min ~ 20 nm	170 W / 7.8 mTorr / 0% O ₂ / 0.5 min ⇒ 170 W / 7.8 mTorr / 4.8% O ₂ / 30 min
11/02	W4	Quartz, 1x1 cm ² 80 C	TiO ₂ , 200W / 3 mTorr / 10% O ₂ / 5 min ~ 25 nm	170 W / 6 mTorr / 4.8% O ₂ / 30 min
11/0	W5	Quartz, 1x1 cm ² 140 C	TiO ₂ , 200W / 3mTorr / 10% O ₂ / 5min ~ 25 nm	170 W / 6 mTorr / 4.8% O ₂ / 30 min
11/08	W6	Quartz, 1x1 cm ² 50 C	TiO ₂ , 200W / 3mTorr / 10% O ₂ / 5min ~ 25 nm	170 W / 9.4 mTorr / 9.1% O ₂ / 30 min
11/11	W7	Quartz, 1x1 cm ² 32 C	TiO ₂ , 200W / 3mTorr / 10% O ₂ / 5min ~ 25 nm	170 W / 6 mTorr / 9.1% O ₂ / 30 min
11/11	W8	Quartz, 1x1 cm ² 32 C	TiO ₂ , 200W / 3mTorr / 10% O ₂ / 4min ~ 20 nm	170 W / 7.8 mTorr / 9.1% O ₂ / 30 min
11/12	W9	Quartz, 1x1 cm ² 32 C	TiO ₂ , 200W / 3mTorr / 10% O ₂ / 5min ~ 25 nm	170 W / 7.8 mTorr / 2.5% O ₂ / 30 min
11/16	W10	Quartz, 1x1 cm ² 30 C	TiO ₂ , 200W / 3mTorr / 10% O ₂ / 5min ~ 25 nm	170 W / 7.8 mTorr / 3.5% O ₂ / 30 min
11/16	W11	Quartz, 1x1 cm ² 30 C	TiO ₂ , 200W / 3mTorr / 10% O ₂ / 5min ~ 25 nm	170 W / 6 mTorr / 9.1% O ₂ / 15 min
11/16	W12	Quartz, 1x1 cm ² 26 C	TiO ₂ , 200W / 3mTorr / 10% O ₂ / 5min ~ 25 nm	170 W / 7.8 mTorr / 2% O ₂ / 30 min
11/19	W13	Quartz, 1x1 cm ² 80 C	TiO ₂ , 200W / 3mTorr / 10% O ₂ / 5min ~ 25 nm	170 W / 7.8 mTorr / 2% O ₂ / 30 min
	W14	Quartz, 1x1 cm ²	TiO ₂ , 200W / 3mTorr / 10% O ₂ / 5min ~ 25 nm	170 W / 6 mTorr / 7.8% O ₂ / 30 min
	W15	Quartz, 1x1 cm ²	TiO ₂ , 200W / 3mTorr / 10% O ₂ / 5min ~ 25 nm	170 W / 6 mTorr / 10.3% O ₂ / 30 min
	W16	Quartz, 1x1 cm ²	TiO ₂ , 200W / 3mTorr / 10% O ₂ / 5min ~ 25 nm	170 W / 5 mTorr / 10.3% O ₂ / 30 min
Wafer1		Quartz, 4"	TiO ₂ , 200W / 3mTorr / 10% O ₂ / 5min ~ 25 nm	170 W / 6 mTorr / 10.3% O ₂ / 30 min O₂ addition was 100s delayed
Wafer2		Quartz, 4"	TiO ₂ , 200W / 3mTorr / 10% O ₂ / 5min ~ 25 nm	170 W / 6 mTorr / 10.3% O ₂ / 30 min
Wafer3		Quartz, 4"	TiO ₂ , 200W / 3mTorr / 10% O ₂ / 5min ~ 25 nm	170 W / 6 mTorr / 10.3% O ₂ / 30 min
Wafer4		Quartz, 4"	TiO ₂ , 200W / 3mTorr / 10% O ₂ / 5min ~ 25 nm	170 W / 6 mTorr / 7.8% O ₂ / 30 min
Wafer5		Quartz, 4"	TiO ₂ , 200W / 3mTorr / 10% O ₂ / 5min ~ 25 nm	170 W / 6 mTorr / 11.5% O ₂ / 30 min
	W17	Quartz	TiO ₂ , 200W / 3mTorr / 10% O ₂ / 5min ~ 25 nm	170 W / 6 mTorr / 11.5% O ₂ / 30 min

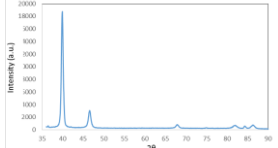
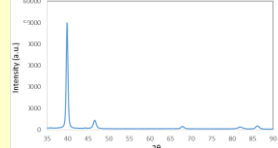
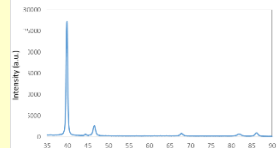
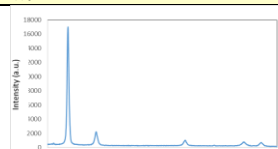
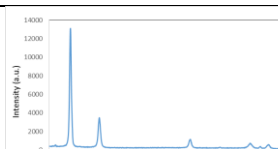
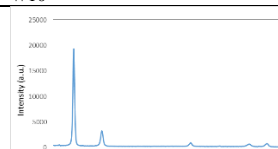
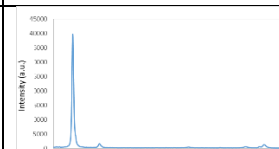

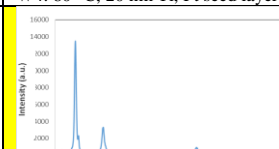
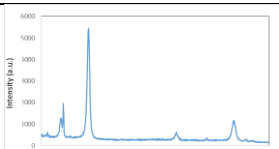
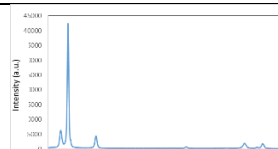
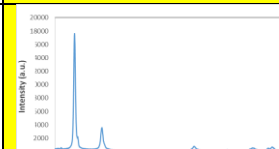


Appendix 2

	9.4 mTorr	7.8 mTorr		6 mTorr
2%		 W13 80 °C	 W12	
2.5 %			 W9	
3.5 %			 W10	
4.8 %	 W1.5	 W3 80 °C, 20 nm Ti, Pt seed layer	 W2 20 nm Ti, Pt seed layer	 W5 140 °C  W4 80 °C, 20 nm Ti, Pt seed layer
7.8 %				 W14
9.1 %	 W6 50 °C		 W8	 W7
10.3 %				 W15
11.5 %				 W17

POST ANNEAL MEASUREMENTS

	9.4 mTorr	7.8 mTorr	6 mTorr
2%		 <p>W13: 80 °C</p>	 <p>W12</p>
2.5 %			 <p>W9</p>
3.5 %			 <p>W10</p>
4.8 %	 <p>W1.5</p>	 <p>W3: 80 °C, 20 nm Ti, Pt seed layer</p>	 <p>W5: 140 °C</p>
7.8 %			 <p>W4: 80 °C, 20 nm Ti, Pt seed layer</p>
9.1 %	 <p>W6, 50 °C</p>	 <p>W8</p>	 <p>W7</p>
10.3 %			 <p>W15</p>
11.5 %			 <p>W17</p>

PRE-ANNEAL MEASUREMENTS

	9.4 mTorr	7.8 mTorr		6 mTorr
2%		 W13: 80 °C	 W12	
2.5%			 W9	
3.5%			 W10	
4.8%	W1.5	 W3: 80 °C, 20 nm Ti, Pt seed layer	 W2: 20 nm Ti, Pt seed layer	 W5: 140 °C  W4: 80 °C, 20 nm Ti, Pt seed layer
7.8%				 W14
9.1%	 W6, 50 °C		 W8	 W7
10.3%				 W15
11.5%				 W17